Estimating Elastic Properties of Tissues from Standard 2D Ultrasound Images

Jan Kybic[a] and Daniel Smutek[b]

[a]Center for Machine Perception, Faculty of Electrical Engineering, Czech Technical University, Prague, Czech Republic
[b]Faculty of Medicine I, Charles University, Prague, Czech Republic

ABSTRACT

We propose a way of measuring elastic properties of tissues in-vivo, using standard medical image ultrasound machine without any special hardware. Images are acquired while the tissue is being deformed by a varying pressure applied by the operator on the hand-held ultrasound probe. The local elastic shear modulus μ is either estimated from a local displacement field reconstructed by an elastic registration algorithm, or both the modulus μ and the displacement are estimated simultaneously. The relation between modulus and displacement is calculated using a finite element method (FEM). The estimation algorithms were tested on both synthetic, phantom and real subject data.

Keywords: Elastography, medical ultrasound, elastic modulus, weak form, finite element method, tissue, inverse problem.

1. INTRODUCTION

Knowing elastic properties of tissues can be very useful for diagnostics as well as for biomechanical modeling. It is known that many kind of carcinoma are harder than the surrounding tissue.[1–3] Elastography, (or elasticity imaging)[4,5] aims at detecting and imaging the corresponding changes of elasticity parameters, most often the Lamé constants μ and λ, or equivalently the Young modulus E and the Poisson ratio ν.

Elastography usually employs a variety of relatively sophisticated and costly technical means. The tissue is compressed statically with a dedicated instrument and the applied force distribution and displacement is carefully measured. Alternatively, transient[6] or harmonic waves[7] are sent through the tissue by a mechanical device or using high-energy ultrasound. The displacement inside the tissue is accurately measured using magnetic resonance (MRI),[8,9] by laser interferometry, or from the ultrasound probe signal (RF signal) sampled at very high frequency.[10,11]

In order to make elastography more widely accessible, we propose to recover the elastic properties of tissues using standard medical image ultrasound machine, without any special hardware. The tissue is deformed by varying the pressure applied by the operator on the transducer in a quasi-static mode.

It turns out that elastic modulus estimation is an ill-posed problem even if good 3D measurements of internal displacements are available and the applied forces are known. Moreover so if, as in our case, the measurements are noisy and incomplete. Thus, many assumptions are unavoidable in order to simplify the problem.

We propose to solve the task as an inverse problem by searching for such μ, so that the corresponding displacement field explains as well as possible the difference between a pair of observed images at slightly different compression levels. The displacement field and the elastic modulus are sought for simultaneously.

We learnt only after the initial submission of this manuscript, that a similar idea has been proposed by Gokhale *et al.*,[12] based on the same previous work describing the adjoint approach[13] to Lagrangian gradient calculation. Here we apply the new algorithm to a number of test cases, ranging from synthetic data to images of a human subject. We describe the method in detail and compare it with a set of alternatives. Compared to Gokhale *et al.*,[12] we work in a much less constrained setting (the applied force and boundary conditions are not known), and our data is noisier and has significantly lower resolution.

email: kybic@fel.cvut.cz, tel: +420 2 2435 5721

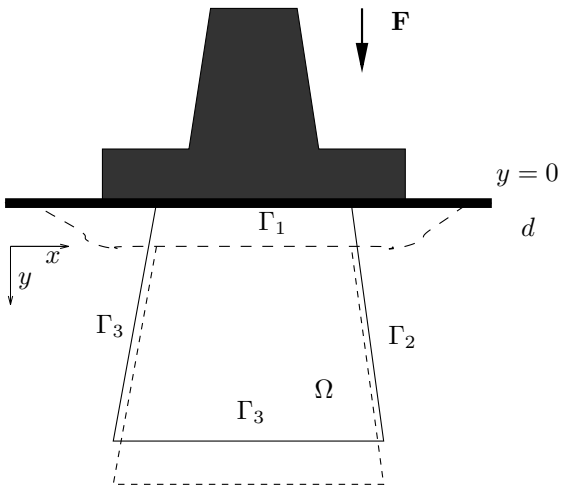

Figure 1. The tissue is deformed by varying the pressure on the ultrasound probe. (Dashed lines show the position of the skin and the sensed region after the probe is shifted downward by a distance d.)

2. METHODS

2.1. Problem description

An ultrasound probe (transducer) is placed on a skin. A sequence of 2D images is automatically acquired while a variable force is applied on the probe in the imaging plane and perpendicularly to the skin, compressing the tissue. Two images f and g of the region Ω with slightly different compression levels of the tissue are selected.

2.2. Assumptions

We would like to determine the elastic tissue properties from the images f and g. However, we clearly do not have enough data to solve the reconstruction problem in all its generality. We will therefore have to simplify it by accepting the following assumptions and approximations:

1. The probe motion is considered a pure translation in the y direction by a distance d. We can then conveniently work in the coordinate system connected with the probe, since the translation will not change the elasticity equations.
2. The displacement is sufficiently small so that linear approximations hold. In practice, the displacement must be at least of the order of several pixels, to be discernible.
3. The displacement is sufficiently slow so that the material is in the equilibrium state.
4. We assume that the material is *isotropic* and *incompressible*, i.e. $\lambda = \infty$, $\nu = 0.5$. This reduces the set of parameters to identify to one, the Lamé parameter μ, also called the shear modulus G.
5. The material is in the state of *plane strain*, i.e. all the out of plane strains (displacements) are assumed zero. This amounts to the assumption that the tissue properties are constant perpendicularly to the imaging plane.

2.3. Governing equations

Let $\mathbf{u} : \mathbb{R}^2 \to \mathbb{R}^2$ be the displacement field between images f and g, i.e., $\mathbf{u}(\mathbf{x}_f) = \mathbf{x}_g - \mathbf{x}_f$, where $\mathbf{x}_f$ resp. $\mathbf{x}_g$ are coordinates of a given tissue point in images f and g, in the image (and probe) coordinate system. Under the above mentioned assumptions the equilibrium equations are[4, 13]:

$$\left.\begin{aligned} -\nabla p + \nabla \cdot \left(2\mu \nabla^s \mathbf{u}\right) &= \mathbf{0} \\ -\nabla \cdot \mathbf{u} &= 0 \end{aligned}\right\} \quad \text{in } \Omega \tag{1}$$

where p is a pressure, positive for compression, and $\boldsymbol{\varepsilon} = \nabla^s \mathbf{u} = \frac{1}{2}(\nabla \mathbf{u} + \nabla \mathbf{u}^T)$ is the symmetric strain tensor.

To obtain a well-posed problem $\mu \mapsto \mathbf{u}$ it is essential to complement the equations (1) with corresponding boundary conditions on the entire boundary $\Gamma = \bigcup_{i=1}^{4} \Gamma_i$ (see Figure 1). Clearly, the displacement on the top edge Γ_1 is 0 in the moving coordinate system, since the tissue there follows the movement of the probe. For lack of better information, we are forced to make the following assumptions on the remaining edges: on the bottom edge we prescribe a vertical force of unknown magnitude H, constant on Γ_3; the remaining edges are considered free, with no external force acting on them. Hence, the boundary conditions are:

$$\begin{aligned} \mathbf{u} &= \mathbf{0} \qquad \text{on } \Gamma_1 \\ \underbrace{\big(-\nabla p \mathbf{1} + \big(2\mu \nabla^s \mathbf{u}\big)\big)}_{\text{stress } \boldsymbol{\sigma}} \cdot \mathbf{n} &= \begin{cases} \mathbf{0} & \text{on } \Gamma_2 \cup \Gamma_4 \\ H \mathbf{e}_y & \text{on } \Gamma_3 \end{cases} \end{aligned} \tag{2}$$

where $\mathbf{n}$ is the unit outward normal vector on Γ and $\mathbf{e}_y = [0\ 1]^T$. Boundary conditions (2) make the forward problem $\mu, H \mapsto \mathbf{u}$ described by (1) well-posed and unique (for strictly positive μ).[14] Introducing a separate variable p is necessary to obtain a well conditioned problem and to avoid mesh locking.

2.4. Weak formulation

To get rid of the second order derivatives, relax the regularity conditions, and improve numerical stability, we convert the strong formulation (1), (2) to an equivalent weak one.[13] The following equation must hold for all sufficiently regular and integrable test functions $\mathbf{w}$ and q such that $\mathbf{w} = \mathbf{0}$ on Γ_1.

$$\underbrace{\int_\Omega 2\mu \nabla^s \mathbf{u} : \nabla^s \mathbf{w} - (\nabla \cdot \mathbf{w}) p - (\nabla \cdot \mathbf{u}) q \, \mathrm{d}\Omega}_{A\left(\mu;(\mathbf{u},p),(\mathbf{w},q)\right)} = \underbrace{H \int_{\Gamma_3} \mathbf{w} \cdot \mathbf{n} \, \mathrm{d}\Gamma}_{b(\mathbf{w},H)} \tag{3}$$

2.5. Finite element method

The domain Ω is triangulated to form a mesh $\mathcal{M}^h$ with a characteristic size h; see Figure 2 for an example. Note that the domain Ω does not have to be rectangular, this is useful for example for sector probes, where trapezoidal zone is more appropriate. Following the Galerkin principle, all functions in (3) are projected onto a finite-dimensional vector space with P1 (C^1, linear on each mesh triangle) basis functions $\boldsymbol{\varphi}_i$ for $\mathbf{u}, \mathbf{w}$, and P0 (constant on each triangle) basis functions ψ_j for p, q. For the approximated functions we have

$$\begin{aligned} \mathbf{u}^h &= \sum_i u_i \boldsymbol{\varphi}_i \\ p^h &= \sum_j p_j \psi_j \end{aligned} \tag{4}$$

and equivalently for $\mathbf{w}$ and q. Given μ, H, we can form a sparse and symmetric set of equations for $\mathbf{u}^h$, p^h.

$$A\big(\mu; (\mathbf{u}^h, p^h), (\boldsymbol{\varphi}_i, \psi_j)\big) = b(\boldsymbol{\varphi}_i, H) \quad \text{for all } \boldsymbol{\varphi}_i,\ \psi_j \tag{5}$$

The system (5) can be efficiently solved by some iterative method, such as the method of conjugated gradients.[15,16] As the mesh size h converges to 0, e.g. by decimating the mesh, the FEM solution $(\mathbf{u}^h, p^h)$ is guaranteed to converge[14] to the true continuous solution of (3). To impose the zero displacement condition (2) on Γ_1, the weights u_i for nodes on Γ_1 are identically set to zero and not solved for.

2.6. Image registration

A general purpose elastic image registration algorithm such as[17,18] can be used to recover the displacement field $\mathbf{u}$ from the image pair f, g. However to efficiently couple the estimated $\mathbf{u}$ with the finite element model, it is

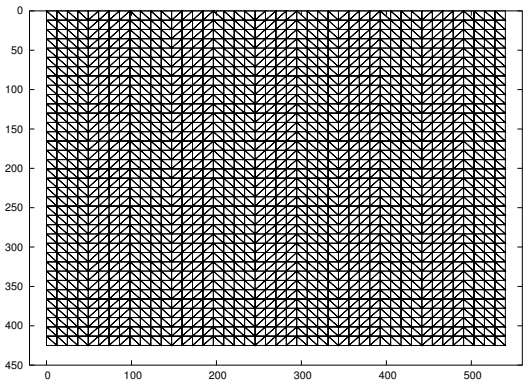

Figure 2. Example mesh for the domain Ω.

advantageous to find $\mathbf{u}$ directly in the appropriate P1 space (4). We decided to minimize an image similarity criterion

$$J_s(\mathbf{u}) = J'_s\big(f, T_\mathbf{u} g\big) \tag{6}$$

with a fixed image f and a moving image g, both grayscale (scalar), where $T_\mathbf{u} g$ is a warped version of image g. We use linear interpolation and zero boundary conditions to evaluate

$$T_\mathbf{u} g(\mathbf{x}) = g\big(\mathbf{x} + \mathbf{u}(\mathbf{x})\big)$$

We use a normalized SSD criterion

$$J'_s(f, T_\mathbf{u} g) = \frac{1}{2} \frac{\sum_{\mathbf{i}\in I} \big(T_\mathbf{u} m_g\big)(\mathbf{i})\; m_f(\mathbf{i})\; \Big(\big(T_\mathbf{u} g\big)(\mathbf{i}) - f(\mathbf{i})\Big)^2}{\sum_{\mathbf{i}\in I} \big(T_\mathbf{u} m_g\big)(\mathbf{i})\; \big(T_\mathbf{u} g\big)(\mathbf{i})^2 + m_f(\mathbf{i}) f(\mathbf{i})^2}$$

where I is the set of pixel coordinates in the image and m_f and m_g are masks, determining the region of interest. This criterion is invariant to image intensity scale changes and largely insensitive to changes of overlap. Normally, we use $m_f = m_g = 1_\Omega$ (1 in Ω and zero outside).

A registration algorithm consists of minimizing $J(\mathbf{u})$ with respect to $\mathbf{u}$ described by (4), in a multiresolution fashion. Let us call the result $\mathbf{u}_r$. We use a gradient descent algorithm, with quadratic step-size estimation.[18–20]

2.7. Strain imaging

Once $\mathbf{u} \approx \mathbf{u}_r$ is known, we can calculate the strain $\boldsymbol{\varepsilon} = \nabla^s \mathbf{u}$ and show it. This is a popular method called strain imaging[4] that provides nice and informative images provided that $\mathbf{u}$ is known precisely (see Figure 4, cases 1–3). Unfortunately, due to the derivative operator ∇^s, the strain image quality deteriorates dramatically if the $\mathbf{u}$ estimate is noisy. It is almost always the case when $\mathbf{u}$ is obtained by registration (see Figure 4, cases 4–5), except when high-quality MRI or ultrasound RF (radio-frequency) data is available.[10,11] Assuming that the strain is principally in the y-direction, we have $\mu \propto 1/\varepsilon_{yy}$. Strain imaging is denoted as Algorithm A in Section 3.

2.8. Direct reconstruction

With known $\mathbf{u} \approx \mathbf{u}_r$, it is also possible[8,21] to solve (1), (2) for μ. To this end, we represent μ in the P1 basis. It leads to a sparse system of linear equations. However, the mapping $\mathbf{u} \mapsto \mu$ is not unique[22] in a non-trivial way.[23] In practical terms we observe that the system matrix is singular or ill-conditioned. Imposing values of μ along the boundary is possible but still leads to an ill-posed (numerically unstable) inverse problem[23] and to completely wrong results when the boundary conditions are incorrect. Neither minimum norm reconstruction is satisfactory; see Figure 3 for an example.

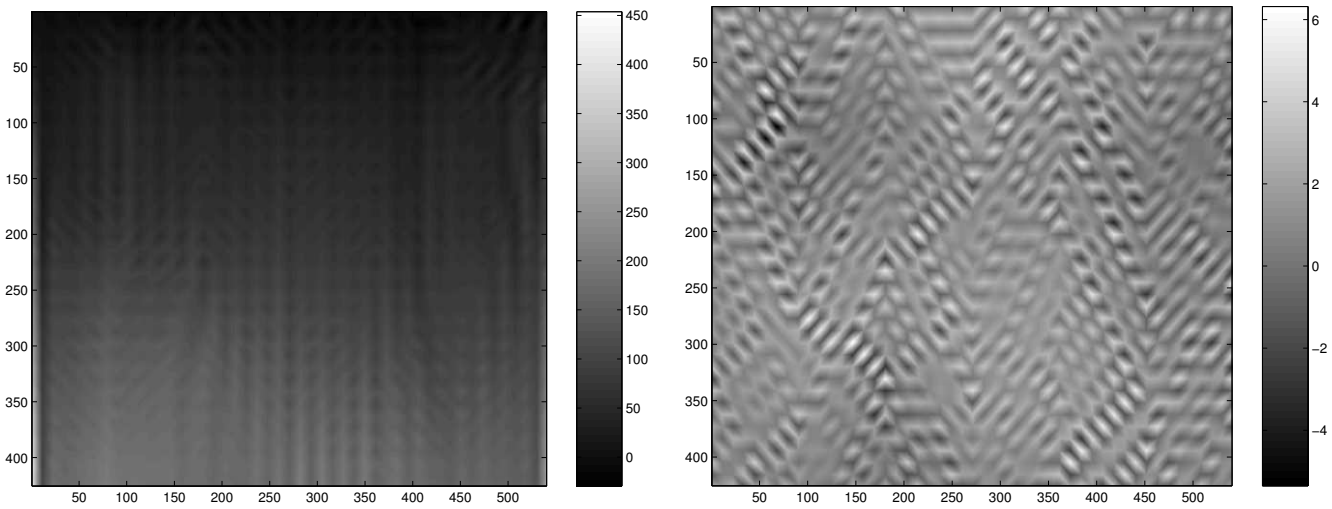

Figure 3. Examples of the instabilities of algebraic reconstruction for μ with imposed constant on the top edge (left image) and minimum norm solution (right image), from calculated displacement data for image pair 1 (Figure 4, first row). Using correct boundary values, the result is indistinguishable from the correct solution (Figure 4, first row, middle column).

2.9. Sequential estimation

To accommodate for noise in the displacement estimate $\mathbf{u}_r$, we can minimize the discrepancy

$$J_d(\mathbf{u}) = \|\mathbf{u} - \mathbf{u}_r\|_{L_2}^2$$

with respect to μ, H, under the constraints (1), (2). To obtain an unconstrained problem, we form a Lagrangian

$$L\big(\mu, H; (\mathbf{u}, p), (\mathbf{w}, q)\big) = J(\mathbf{u}) - A\big(\mu; (\mathbf{u}, p), (\mathbf{w}, q)\big) + b(\mathbf{w}, H) \tag{7}$$

where we interpret the test functions $(\mathbf{w}, q)$ as Lagrange multipliers. The minimization of L with respect to (μ, H) is handled by a gradient descent algorithm where the gradient $D_{(\mu,H)}L$ is calculated by an adjoint approach[13]:

1. solve for $(\mathbf{u}, p)$: $\quad D_{(\mathbf{w},q)}L = 0 \quad \Rightarrow \quad \forall(\delta\mathbf{w}, \delta q);\, A\big(\mu; (\mathbf{u}, p), (\delta\mathbf{w}, \delta q)\big) = b(\delta\mathbf{w}, H)$
2. solve for $(\mathbf{w}, q)$: $\quad D_{(\mathbf{u},p)}L = 0 \quad \Rightarrow \quad \forall(\delta\mathbf{u}, \delta p);\, A\big(\mu; (\delta\mathbf{u}, \delta p), (\mathbf{w}, q)\big) = D_{\mathbf{u}}\, J(\mathbf{u})\, \delta\mathbf{u}$
3. evaluate $D_{(\mu,H)}L$ $\quad D_\mu L \delta\mu = -A\big(\delta\mu; (\mathbf{u}, p), (\mathbf{w}, q)\big) = -2\int_\Omega \delta\mu \nabla^s\mathbf{u} : \nabla^s\mathbf{w}\, \mathrm{d}\Omega$

$$D_H L\, \delta H = b(\mathbf{w}, \delta H) = \delta H \int_{\Gamma_3} \mathbf{w}\cdot\mathbf{n}\, \mathrm{d}\Gamma$$

The first step is equivalent to solving forward problem (3). The second step solves the dual problem and thanks to the symmetry of A, it is completely equivalent to the forward one. Note that all equations hold if H and μ are multiplied by the same constant. Optimizing for both H and μ simultaneously is therefore ill-conditioned. Nevertheless, we found it useful to to briefly optimize for H at the beginning of each multiresolution level with μ fixed; after that we optimize for μ. This is known as Algorithm B in Section 3.

2.10. Unidirectional discrepancy

The resolution of the ultrasound sensor and thus also the accuracy of the displacement estimation is much better in the y-direction. Moreover, the load is predominantly in the y-direction, too. Therefore, we replace the total discrepancy J_d with a criterion considering only the y-component[13]:

$$J_y(\mathbf{u}) = \|(\mathbf{u} - \mathbf{u}_r)\cdot\mathbf{e}_y\|_{L_2}^2$$

This is known as Algorithm C in Section 3.

2.11. Simultaneous estimation

The disadvantage of the two-stage sequential estimation (first $\mathbf{u}$, then μ) is precisely that the two stages do not communicate. If the image quality is poor, the registration algorithm may well propose a displacement field inconsistent with any elastic deformation. It will interpolate the displacement in detail-free zones without regard for the equations governing elasticity. On the other hand, the modulus μ estimator will have equal confidence in the displacement field at all points, which is suboptimal. Hence the idea of simultaneous estimation of $\mathbf{u}, p, \mu, H$. We replace a reference displacement field based criterion J_y or J_d, by a criterion J_s (6). This way we search for a deformation that best explains the differences between images f and g while respecting the elasticity constraints (1). The corresponding Lagrangian is

$$L\big(\mu, H; (\mathbf{u}, p), (\mathbf{w}, q)\big) = J_s(\mathbf{u}) - A\big(\mu; (\mathbf{u}, p), (\mathbf{w}, q)\big) + b(\mathbf{w}, H) \tag{8}$$

To overcome the local minima problems with respect to $\mathbf{u}$, a multiresolution approach is used and the images are initially smoothed with a low-pass filter. This is known as Algorithm D in Section 3.

2.12. Regularization on μ

To reduce the indeterminacy of μ we introduce a regularization criterion based on our *a priori* assumption that μ varies little within each region of a single tissue type. There can be discontinuities of μ on boundaries between different types of tissue that we want to preserve. We therefore chose to minimize the L_1 norm of the gradient[24]:

$$J_r = \int_\Omega \|\nabla \mu\| \ \mathrm{d}\Omega \tag{9}$$

The Lagrangian (7) resp. (8) then becomes

$$L\big(\mu, H; (\mathbf{u}, p), (\mathbf{w}, q)\big) = J(\mathbf{u}) + \alpha J_r(\mu) - A\big(\mu; (\mathbf{u}, p), (\mathbf{w}, q)\big) + b(\mathbf{w}, H) \tag{10}$$

where the data attachment term $J(\mathbf{u})$ can be J_d, J_y, or J_s, and α is the regularization factor. The algorithm to calculate $D_{(\mu,H)}L$ for (10) based on the stationarity conditions is consequently modified as follows:

1. solve for $(\mathbf{u}, p)$: $\quad D_{(\mathbf{w},q)}L = 0 \quad \Rightarrow \quad \forall(\delta\mathbf{w}, \delta q); A\big(\mu; (\mathbf{u}, p), (\delta\mathbf{w}, \delta q)\big) = b(\delta\mathbf{w}, H)$
2. solve for $(\mathbf{w}, q)$: $\quad D_{(\mathbf{u},p)}L = 0 \quad \Rightarrow \quad \forall(\delta\mathbf{u}, \delta p); A\big(\mu; (\delta\mathbf{u}, \delta p), (\mathbf{w}, q)\big) = D_{\mathbf{u}}\, J(\mathbf{u})\, \delta\mathbf{u}$
3. evaluate $D_{(\mu,H)}L$ $\quad D_\mu L\, \delta\mu = \alpha D_\mu J_r \delta\mu - A\big(\delta\mu; (\mathbf{u}, p), (\mathbf{w}, q)\big) = \alpha D_\mu J_r \delta\mu - 2\int_\Omega \delta\mu \nabla^s\mathbf{u} : \nabla^s\mathbf{w} \ \mathrm{d}\Omega$

$$D_H L\, \delta H = b(\mathbf{w}, \delta H) = \delta H \int_{\Gamma_3} \mathbf{w} \cdot \mathbf{n} \ \mathrm{d}\Gamma$$

For our images, we used $\alpha = 10^{-5} \sim 10^{-7}$.

3. EXPERIMENTS

3.1. Images

We have prepared a set of five image pairs, synthetic and real (acquired), to test all aspects of the reconstruction algorithms (see Figure 4):

1. An artificially generated image with texture deformed with a displacement field corresponding to a known modulus with a single inclusion.
2. An artificially generated texture-less image deformed with the same displacement field as for image pair 1.
3. An acquired ultrasound image of a phantom deformed with a calculated displacement field. The modulus distribution was chosen so that the calculated displacement field is similar to an observed one.

4. A pair of acquired ultrasound images of a phantom for slightly different levels of applied force. The true modulus is unknown but we suppose it is similar to modulus used to generate image pair 3.

5. A pair of acquired ultrasound images of a normal thyroid gland for different levels of applied force. Nothing is known about the true modulus in this case.

Test images 1–3 (Figure 4, left column) were deformed by an elastic deformation corresponding to applying small vertical compression and chosen modulus distribution (Figure 4, middle column), forming test pairs. The maximum displacement was $5 \sim 10$ pixels, i.e. $1 \sim 2\,\%$ strain. Test image pairs 4–5 were acquired on an ultrasound scanner by varying the pressure.

3.2. Algorithms

The image pairs were processed by the following four algorithms to obtain estimates of the distribution of modulus μ, respectively strain $\boldsymbol{\varepsilon}$:

A. Direct strain estimation from the calculated true displacements or from displacements recovered by the elastic registration algorithm. Described in Section 2.7.

B. Estimating the modulus by minimizing the discrepancy between the calculated displacement field and the displacement field recovered by the elastic registration algorithm. Described in Section 2.9.

C. Minimizing the discrepancy as above but taking only the vertical (y) component into account. Described in Section 2.10.

D. Simultaneously estimating the modulus and the displacement. Described in Section 2.11.

3.3. Evaluation

Vertical strain images (ε_{yy}, Algorithm A) are shown in Figure 4 (right column). Observe that they correspond very well to the true modulus images for pairs 1–3, where displacement is known exactly. Unfortunately, for displacements estimated from a pair of ultrasound images (4–5), the strain images are extremely noisy, hence unusable. We are not including the results by direct reconstruction (Section 2.8), because it performed badly on our data.

Figure 5 permits to evaluate the quality of the different registration methods. The left column shows the original difference between the two images in the pair. The middle column shows the difference after registration by minimizing J_s (Section 2.6) without regard to the elasticity constraints. The differences were sometimes left uncorrected at image borders due to a mask used. The right column shows the differences after simultaneous registration and modulus estimation (Algorithm D, Section 2.11). We observe that both registration algorithm perform well. Moreover, there is almost no penalty for imposing the elasticity constraints.

Figure 6 shows the modulus distributions estimated by the three remaining algorithms presented (B - Section 2.9, C - Section 2.10, D - Section 2.11) for the 5 test image pairs. For images 1–3, you can compare the results with the ground truth (Figure 4). Clearly, algorithm B is the worst, most likely because the recovered deformation field is not consistent with the elasticity constraints. The best of the remaining two is algorithm D — simultaneous registration and modulus estimation. It succeeds in recovering the modulus reasonably well in all three synthetic cases (1–3).

On the real phantom data the results of the algorithm D are average — the inclusions (in image 4) are only barely discernible and there are artifacts (namely in the upper left and upper right corners). We think that it is because of the bad quality of the phantom image data: there are shadows in the images and the plane strain condition is probably violated due to a small size and half-spherical shape of the phantom.

The quality of the results on the thyroid data is difficult to evaluate since we have no ground truth. However, the recovered modulus seems to be consistent with visual observation and medical experience.

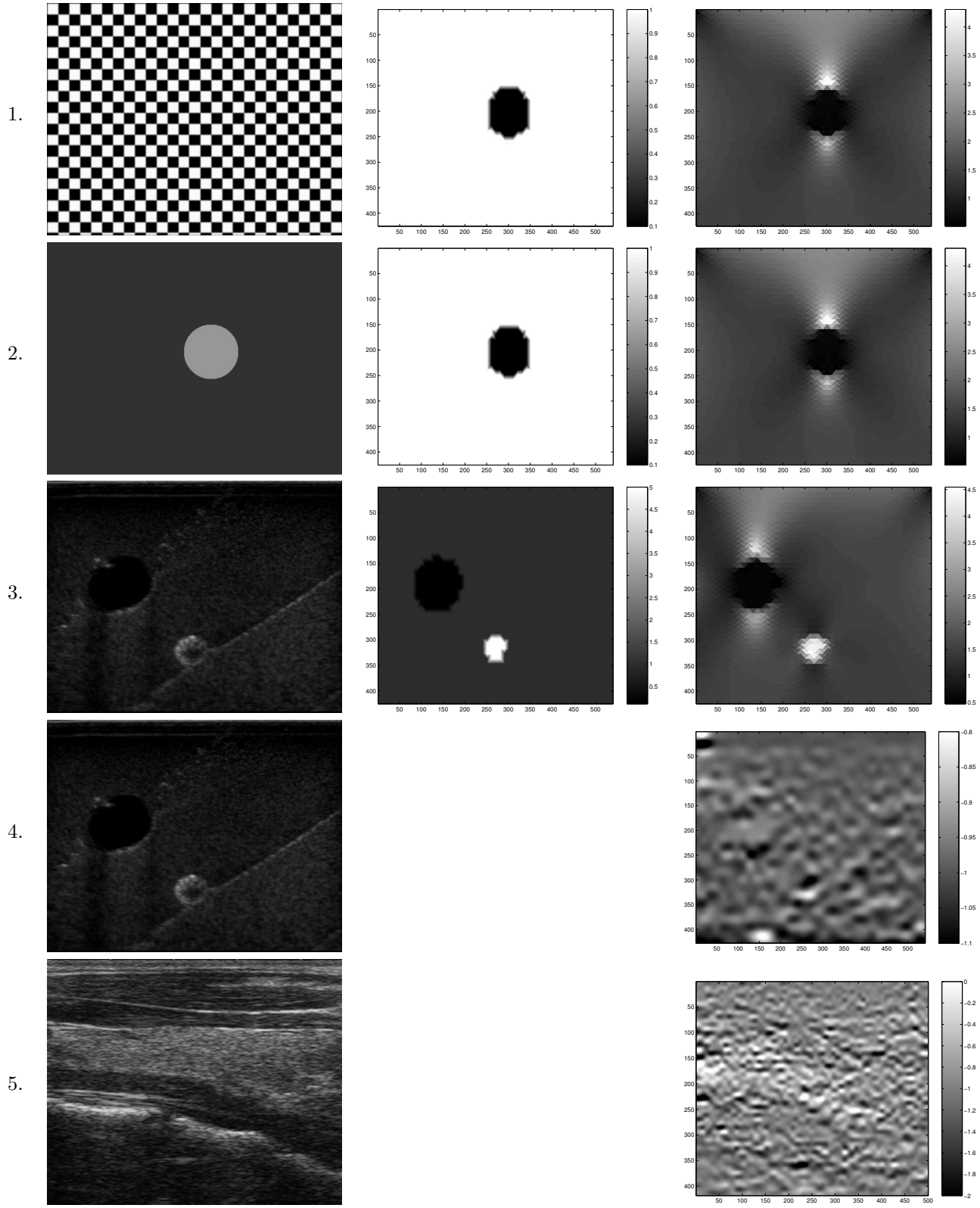

Figure 4. The test images as described in Section 3.1 (left column). When available (images 1-3), we show also the chosen modulus (μ) distribution (middle column), and corresponding strain image (right column) derived from the calculated displacement. For images 4 and 5, where ground truth modulus is not available, we show strain images derived from the displacement field found by the registration algorithm.[18] Vertical component of the strain is shown.

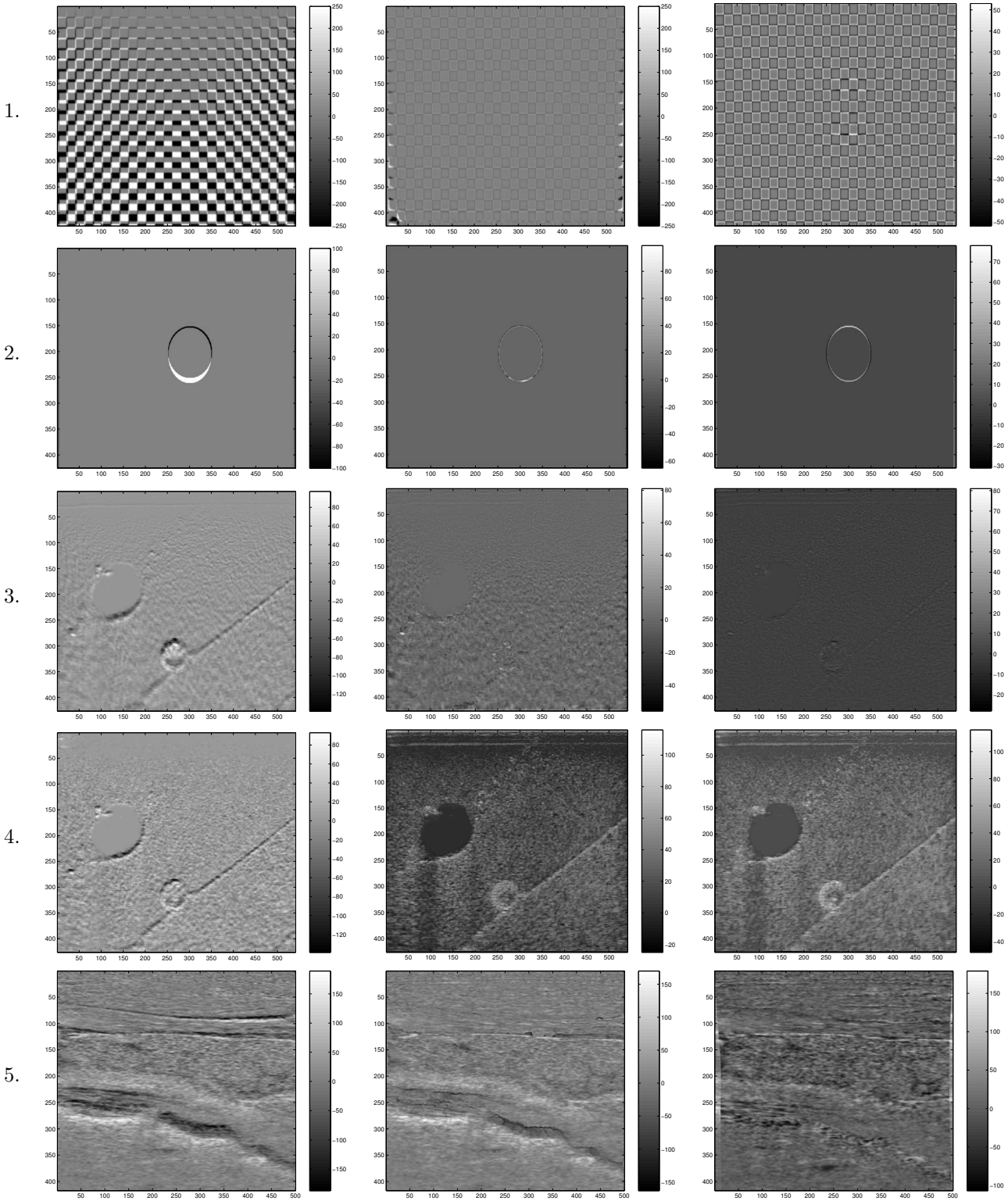

Figure 5. The difference images (left column) for the 5 image pairs. Difference after unconstrained registration (Section 2.6, middle column) and after simultaneous registration and modulus estimation (Section 2.11, right column).

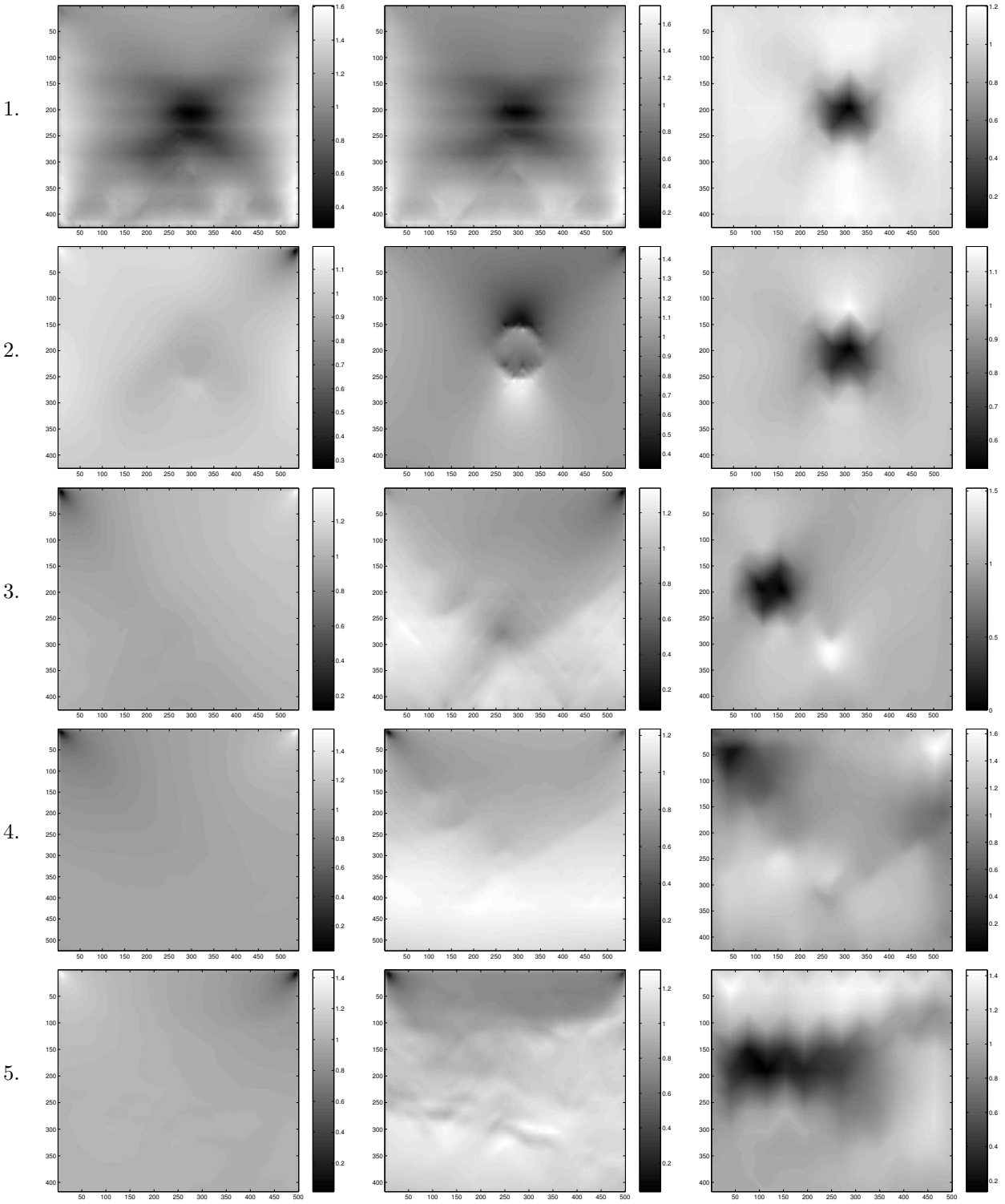

Figure 6. The modulus μ estimated by various algorithms for all test pairs: Estimation by minimizing discrepancy by previously recovered displacement field (algorithm B, Section 2.9, left column), by minimizing only the $y-$component of the discrepancy (algorithm C, Section 2.10, middle column), and by simultaneously registering the images and estimating the modulus (algorithm D, Section 2.11, right column).

3.4. Material, implementation and timings

Ultrasound images were acquired on a standard Philips Envisor ultrasound scanner. We have used the Gammex 429 Ultrasound Biopsy Phantom* that mimics normal tissue and contains eleven test objects filled with low or high density gel, simulating lesions (image pairs 3,4). We also recorded images of a normal thyroid gland (image pair 5).

All algorithms were implemented in the Ocaml language and run on a standard PC (Pentium 1.4 GHz). For a 500×400 pixel image the modulus estimation takes about 2 minutes, depending on the desired accuracy and mesh density. We typically use mesh spacing of around 10 pixels per node. The inner-loop conjugated gradient algorithm has prescribed relative accuracy 10^{-6}, the outer gradient descent stops when the relative improvement is smaller than 10^{-3}.

4. CONCLUSIONS

We have described a practical algorithm to solve the inverse elasticity estimation task as a coupled constrained minimization problem consisting of optimizing simultaneously the modulus distribution μ and the displacement field $\mathbf{u}$. As the measurements are never explicitly differentiated, the proposed algorithm is much less sensitive to noise than direct reconstruction approaches. Simultaneous estimation also worked better than estimating μ from the field $\mathbf{u}$ recovered by a general image registration algorithm.

We showed how to choose the assumptions on the forward problem necessary to overcome the lack of data, so that they are at the same time physically plausible and lead to a well-conditioned and numerically stable system. We also pointed out the indeterminacy of μ and hope to alleviate the problem by regularization and good starting estimate choice.

The reconstruction algorithm performed well on several types of synthetic data. However, treating real ultrasound data from a standard medical ultrasound scanner remain a challenge because of its low spatial resolution and high level of noise. Furthermore, it is difficult in hand-held scanning to maintain the imaging plane and the direction of the applied force. We also suspect significant violation of the plane strain condition in our phantom images.

Nevertheless, we believe that by improving both the acquisition and further robustifying the reconstruction, our proposed method of elastographic imaging based solely on a medical ultrasound scanner will produce results comparable to dedicated elastographic instruments.

ACKNOWLEDGMENTS

This work was sponsored by the Grant Agency of the Czech Academy of Sciences, grant IET101050403.

REFERENCES

1. H. T. Liu and L. Z. Sun, "Analytic modeling of breast elastography," *Medical Physics* **30**, pp. 2340–2349, Sept. 2003.
2. W.-C. Yeh, P.-C. Li, Y.-M. Jeng, H.-C. Hsu, P.-L. Kuo, M.-L. Li, P.-M. Yang, and P. H. Lee, "Elastic modulus measurements of human liver and correlation with pathology," *Ultrasound in Medicine & Biology* **28**, pp. 467–474, apr 2002.
3. Yin, Sun, Wang, and M. Vannier, "Modeling of elastic modulus evolution of cirrhotic human liver," *IEEE Trans. Biomed Eng.* **51**, pp. 1854–1856, Oct. 2004.
4. J. Ophir, F. Kallel, T. Varghese, E. Konofagou, S. K. Alam, B. Garra, T. Krouskop, and R. Righetti, "Elastography: Optical and acoustic imaging of acoustic media," *C. R. Acad. Sci. Paris* **2**(8), pp. 1193–1212, 2001. serie IV.
5. M. F. Insana, L. T. Cook, and C. P., "Analytical study of bioelasticity ultrasound systems.," in *Information Processing in Medical Imaging (IPMI)*, K. A., S. M., and T.-P. A., eds., Berlin, 1999.

*`www.gamex.com`

6. J. Lin and J. McLaughlin, "Recovery of the lamé parameter μ in biological tissues," *Inverse Problems* (20), pp. 1–24, 2004.
7. J. R. McLaughlin and Y. J.-R., "Unique identifiability of elastic parameters from time-dependent interior displacement measurement," *Inverse Problems* (20), pp. 24–45, 2004.
8. J. Bishop, A. Samani, J. Sciaretta, and P. D. B., "Two-dimensional MR elastography with linear inversion reconstruction: methodology and noise analysis," *Phys. Med. Biol.* (45), pp. 2081–2091, 2000.
9. H. Liu and P. Shi, "Robust identification of object elasticity," in *Computer Vision and Mathematical Methods in Medical and Biomedical Image Analysis (CVAMIA+MMBIA)*, M. Šonka, A. I. Kakadiaris, and J. Kybic, eds., *Lecture Notes in Computer Science*, pp. 423–435, Springer, Heidelberg, May 2004.
10. S. Srinivasan and J. Ophir, "A zero-crossing strain estimator for elastography," *Ultrasound in Medicine and Biology* **29**, pp. 227–238, Feb. 2003.
11. E. Brusseau, J. Fromageau, N. Rognin, P. Delacharte, and D. Vray, "Local estimation of RF ultrasound signal compression for axial strain imaging: theoretical developments and experimental design," *IEEE Engineering in Medicine and Biology Magazine* **21**, pp. 86–94, jul 2002.
12. P. Barbone, N. Gokhale, M. Richards, A. Oberai, and M. Doyley, "Simultaneous elastic image registration and elastic modulus reconstruction.," in *Proceedings of the 2004 IEEE International Symposium on Biomedical Imaging: From Nano to Macro, Arlington, VA, USA, 15-18 April 2004*, pp. 543–546, IEEE, 2004.
13. A. Oberai, N. Gokhale, and G. Feijóo, "Solution of inverse problems in elasticity imaging using the adjoint method," *Inverse Problems* (19), pp. 297–313, 2003.
14. J. Necas and I. Hlavacek, *Mathematical Theory of Elastic and Elasto-Plastic Bodies*, Elsevier, Amsterdam, 1981.
15. W. H. Press, S. A. Teukolsky, W. T. Vetterling, and B. P. Flannery, *Numerical Recipes in C*, Cambridge University Press, second ed., 1992.
16. R. Barret, M. Berry, T. F. Chan, J. Demmel, J. Donato, J. Dongarra, V. Eijkhout, R. Pozo, C. Romine, and H. van der Vonst, *Templates for the Solution of Linear Systems: Building Blocks for Iterative Methods*, SIAM J. Math. Anal., Philadelphia, 1994. Available from netlib.
17. J. Kybic, P. Thévenaz, A. Nirkko, and M. Unser, "Unwarping of unidirectionally distorted EPI images," *IEEE Transactions on Medical Imaging* **19**, pp. 80–93, February 2000.
18. J. Kybic and M. Unser, "Fast parametric elastic image registration," *IEEE Transactions on Image Processing* **12**, pp. 1427–1442, November 2003.
19. J. Barzilai and J. M. Borwein, "Two point step size gradient method," *IMA J. Numer. Anal.* (8), pp. 141–148, 1988.
20. A. Neculai, "A new gradient descent method for unconstrained optimization." http://www.ici.ro/camo/neculai/anpaper.htm.
21. Y. Zhu, T. J. Hall, and J. Jiang, "A finite element approach for young's modulus reconstruction.," *IEEE Trans. Med. Imaging* **22**(7), pp. 890–901, 2003.
22. P. E. Barbone and J. C. Bamber, "Quantitative elasticity imaging: what can and cannot be inferred from strain images," *Phys. Med. Biol.* (47), pp. 2147–2164, 2002.
23. P. E. Barbone and N. H. Gokhale, "Elastic modulus imaging: on the uniqueness and nonuniqueness of the elastography inverse problem in two dimensions," *Inverse Problems* (20), pp. 283–296, 2004.
24. H. Nagel and W. Enkelmann, "An investigation of smoothness constraint for the estimation of displacement vector fields from image sequences," *IEEE Transactions on Pattern Analysis and Machine Intelligence* **8**, pp. 565–593, 1986.